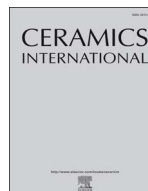




Contents lists available at ScienceDirect

Ceramics International

journal homepage: www.elsevier.com/locate/ceramint

Sheet resistance dependence of fluorine-doped tin oxide films for high-performance electrochromic devices

Kue-Ho Kim^{a,1}, Bon-Ryul Koo^{b,1}, Hyo-Jin Ahn^{a,b,*}

^a Department of Materials Science and Engineering, Seoul National University of Science and Technology, Seoul 01811, South Korea

^b Program of Materials Science & Engineering, Convergence Institute of Biomedical Engineering and Biomaterials, Seoul National University of Science and Technology, Seoul 01811, South Korea

ARTICLE INFO

Keywords:

Films
Electrical properties
Optical properties
Transition metal oxides
Electrochromic performances

ABSTRACT

In the present study, we fabricated fluorine-doped tin oxide (FTO) films with different sheet resistances ($\sim 10 \Omega/\square$, $\sim 6 \Omega/\square$, and $\sim 3 \Omega/\square$) prepared through the adjustment of deposition time during the horizontal ultrasonic spray pyrolysis deposition (HUSPD) and investigated the effect of electrochromic (EC) performances with different sheet resistances of the FTO films used as transparent conducting electrodes. The results demonstrated that, owing to the increased electrochemical activity, the decrease of sheet resistance accelerated switching speeds of the EC devices. However, for the coloration efficiency (CE), the FTO films with the optimum sheet resistance of $\sim 6 \Omega/\square$ exhibited the highest value as compared to the other samples. The improvement of the CE value can be mainly attributed to high transmittance modulation by the uniform surface morphology of the FTO films to reduce interfacial light-scattering between the WO_3 films and FTO films. Therefore, our results provide a valuable insight into the improvement of the performance of the EC devices using the optimum sheet resistance ($\sim 6 \Omega/\square$) of the FTO films.

1. Introduction

With the development of energy-efficient and convenient applications such as smart windows, electronic displays, and adjustable mirrors, electrochromic devices (ECDs), with their unique characteristics of visibility in sunlight, colour variations, and a low operating voltage, have become increasingly important for researchers [1–3]. These devices can accurately control various optical properties (e.g., transparency, absorption, reflection, and colour) under a small electric field, which is typically composed of three functional layers: the cathodic electrochromic (EC) layer, the electrolyte layer, and the anodic EC layer between transparent conducting layers [4,5]. For practical application of ECDs, it is necessary to improve the EC performances including coloration efficiency (CE) and switching speed, which is mainly determined by the components of the ECDs [6]. At this point, improving the performances of transparent conducting layers is an important research direction, as these layers perform a fundamental role in assigning transparency to the ECDs and connecting the devices with the external power supply [7]. Currently, indium tin oxide (ITO) is a representative material used as the transparent conducting layer in optoelectronic applications (touch screens, organic light emitting diodes,

and sensors). ITO is characterized by low resistivity ($< 10^{-3} \Omega \text{ cm}$), high transparency ($> 80\%$), and relatively high work function (4.8 eV) [8,9]. However, ITO also has several critical drawbacks, such as high element cost and vulnerable mechanical and chemical stabilities [8]. In this context, it is imperative to develop alternative materials. Recently, due to its good transparent conducting performance, low cost, and good chemical durability, fluorine-doped SnO_2 (FTO) has received a noticeable interest as a transparent conducting layer for the ECDs or dye-sensitized solar cell [10]. Much effort has been invested into fabricating the FTO films with low sheet resistance or high optical transmittance so that to increase their performances for practical applications. To this end, several methods have been used, including ultrasonic spray pyrolysis deposition (USPD), magnetron sputtering, and chemical vapor deposition [10–12]. Among these methods, USPD has been widely used to form doped or undoped films with superb quantity, especially FTO, which makes it possible to fabricate the film structure on the substrate by pyrolysis of precursor droplets with 1–100 μm in size formed through the ultrasonic atomization [10]. In addition, this method can simply perform the adjustment of transparent conducting performances on the FTO films by controlling the deposition conditions such as deposition temperature, carrier gas, precursor, and additive [13,14]. For

* Corresponding author at: Department of Materials Science and Engineering, Seoul National University of Science and Technology, Seoul 01811, South Korea.

E-mail address: hjahn@seoultech.ac.kr (H.-J. Ahn).

¹ K.-H. Kim and B.-R. Koo contributed equally to this work.

<https://doi.org/10.1016/j.ceramint.2018.02.157>

Received 10 February 2018; Received in revised form 17 February 2018; Accepted 19 February 2018
0272-8842/ © 2018 Elsevier Ltd and Techna Group S.r.l. All rights reserved.

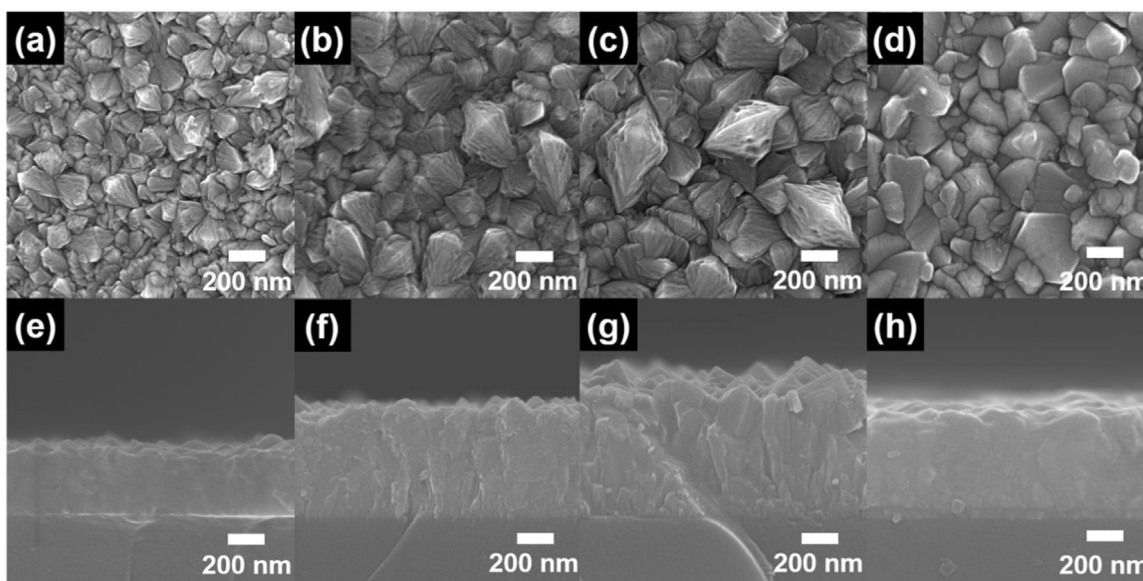


Fig. 1. Top-view and cross-view FESEM images of (a, e) FTO-10 Ω , (b, f) FTO-6 Ω , (c, g) FTO-3 Ω , and (d, h) commercial FTO, respectively.

example, Lin et al. controlled the deposition temperature of the FTO films using the USPD and showed the optimized performances at 400 °C with minimum resistivity of $6.20 \times 10^{-4} \Omega \text{ cm}$ and maximum transmittance of 77.0% [13]. Furthermore, Moholkar et al. performed the FTO deposition by varying concentration of SnCl_4 solution, achieving the maximum values of transparent conducting performances (resistivity of $3.70 \times 10^{-4} \Omega \text{ cm}$ and transmittance of 87.0%) at 0.81 M [14]. However, despite these efforts, convincing evidence on the relationship between the sheet resistance of the FTO films and EC performances has not been reported yet.

In the present study, we prepared the FTO films with three types of sheet resistance ($\sim 10 \Omega/\square$, $\sim 6 \Omega/\square$, and $\sim 3 \Omega/\square$, where \square is cm^2) using horizontal ultrasonic spray pyrolysis deposition (HUSPD) and demonstrated the effect of their sheet resistances on the EC performances by investigating the morphological, structural, chemical, electrical, optical, and electrochemical properties.

2. Experimental details

2.1. Experimental

The FTO films with different sheet resistances were prepared by the HUSPD (Ceon, Nano SPD, TV500, Korea) on the glass substrate (Corning EAGLE XG™). For the preparation of the precursor solution for the FTO deposition, 0.68 M tin chloride pentahydrate ($\text{SnCl}_4 \cdot 5\text{H}_2\text{O}$, SAMCHUN) and ammonium fluoride (NH_4F , Aldrich) were dissolved into de-ionized (DI) water with 5 vol% ethyl alcohol ($\text{C}_2\text{H}_5\text{OH}$, Duksan); to obtain the optimum transparent conducting performance of the FTO films, the mole ratio of F/Sn was fixed at 1.765. After stirring, the resultant precursor solution was placed in a spray container and then the HUSPD was started after maintaining the substrate temperature at 420 °C by ultrasonic atomizer (1.6 MHz). All other deposition conditions during the HUSPD, such as flow rate (15 L/min) of the carrier gas (air), and rotation speed (5 rpm) of the substrate, were maintained constant. To adjust the sheet resistance of the FTO films, the deposition time of the HUSPD was controlled to be 18, 28, and 33 min, resulting in the FTO films with sheet resistance of $\sim 10 \Omega/\square$, $\sim 6 \Omega/\square$, and $\sim 3 \Omega/\square$, respectively (thereafter referred to as FTO-10 Ω , FTO-6 Ω , and FTO-3 Ω , respectively). To measure the EC performance of the FTO films as the transparent conducting electrode (TCE), WO_3 films were used as the working electrode. The WCl_6 sol solution for the preparation of the WO_3 films was obtained by mixing 10 wt% tungsten (VI) chloride (WCl_6 ,

Aldrich) and 2-propanol ($(\text{CH}_3)_2\text{CHOH}$, Aldrich). The resultant sol solution was spin-coated at 2000 rpm for 30 s on all FTO films, which was repeated 2 times. Thereafter, the samples were annealed at 300 °C in air, finally obtaining the EC electrodes consisting of WO_3 films and FTO films (thereafter referred to as WO_3 -FTO-10 Ω , WO_3 -FTO-6 Ω , and WO_3 -FTO-3 Ω , respectively). For comparison, the WO_3 film on the commercial FTO films (WO_3 -commercial FTO) was also fabricated with the sample conditions.

2.2. Characterization

The surface morphology was characterized using field-emission scanning electron microscopy (FESEM, Hitachi S-4800) and atomic force microscopy (AFM, diDimension™ 3100). The crystal structure and chemical state were evaluated using X-ray diffraction (XRD, Rigaku D/Max-2500 diffractometer using $\text{Cu K}\alpha$ radiation) and X-ray photoelectron spectroscopy (XPS, ESCALAB 250 equipped with an Al $\text{K}\alpha$ X-ray source), respectively. The electrical and optical properties were measured by a Hall-effect measurement system (Ecopia, HMS-3000) and ultraviolet-visible (UV-vis) spectroscopy (Perkim-Elmer, Lambda-35), respectively. The electrochemical properties and EC performances were characterized using a potentiostat/galvanostat (PGSTAT302N, FRA32M, Metrohm Autolab B.V., Netherlands), which was performed in the three-electrode system with Ag wire as the reference electrode, Pt wire as the counter electrode, and 1 M LiClO_4 electrolyte at the scan rate of 20 mV/s from -0.7 – 1.0 V. The measurement of *in situ* optical transmittances during coloration and bleaching processes was performed using ultraviolet-visible (UV-vis) spectroscopy (Perkim-Elmer, Lambda-35) in the wavelength at 633 nm.

3. Results and discussion

Fig. 1 shows the top-view and cross-view FESEM images of (a, e) FTO-10 Ω , (b, f) FTO-6 Ω , and (c, g) FTO-3 Ω prepared by different deposition times of the HUSPD, respectively, and (d, h) commercial FTO. As can be seen in the top-view FESEM images (Fig. 1a–d), the FTO films fabricated by the HUSPD have the surface morphology with interlocked pyramid-shaped crystallites throughout the entire surface. Their crystallite sizes enhanced from 182.2–220.0 nm for FTO-10 Ω to 413.7–557.8 nm for FTO-3 Ω , which can be due to the crystallite growth by the increased deposition time of the HUSPD, leading to the

relaxation of inter-grain boundary scattering to improve Hall mobility of the FTO films [14,15]. However, for FTO-3 Ω , due to reorientation effect of FTO crystallites by excessive deposition time, the presence of rod-shaped crystallites is observed among majority of the pyramid-shaped crystallites, which can lead to negative effect on Hall mobility of the FTO films owing to its rough surface morphology [15]. In particular, there is a critical difference of crystallite size distribution ($\Delta R/R$) between FTO-6 Ω and commercial FTO ($\sim 6.0 \Omega/\square$). The distribution of crystallite size is $\sim 12.2\%$ for FTO-6 Ω and $\sim 16.6\%$ for commercial FTO, which means that, as compared to commercial FTO, FTO-6 Ω is made up of uniformly-distributed crystallites. This result can be attributed to the effect of the HUSPD system to uniformly supply the droplets with precursors [10]. Therefore, the uniform film structure of the FTO films prepared by the HUSPD can be an important factor to enhance the performance of the ECDs [16]. As shown in the cross-view FESEM images (Fig. 1e-h), the thickness of the FTO films is in the range of 362.5–371.1 nm for FTO-10 Ω , 619.8–638.8 nm for FTO-6 Ω , 746.6–773.5 nm for FTO-3 Ω , and 588.3–640.1 nm for commercial FTO. These results provide evidence in support of an increase in the thickness with increasing the deposition time of the HUSPD. In addition, from FTO-3 Ω , the rough surface morphology by growth of rod-shaped crystallites can be observed. These phenomena of the SEM results are also confirmed by the AFM results shown in Fig. 2.

Fig. 3 shows the XRD patterns of the FTO films with different sheet resistances as a function of deposition time by HUSPD. All films contain the characteristic diffraction peaks at 26.53° , 33.82° , 37.90° , and 51.72° , which corresponds to the (110), (101), (200), and (211) planes of a tetragonal rutile SnO_2 (space group $P42/mmm$ [136], JCPDS no. 88-0287), respectively. The resultant diffraction peaks exhibit slightly

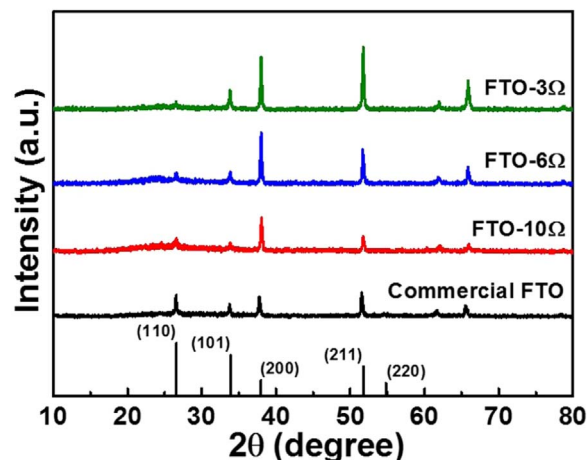


Fig. 3. XRD curves of FTO-10 Ω , FTO-6 Ω , FTO-3 Ω , and commercial FTO.

shifted values to a lower angle as compared to pure SnO_2 (see bottom of Fig. 3). This indicates that the formation of FTO phases is successfully performed as the substitution of a larger F^- (ionic radius 0.133 nm) for smaller O^{2-} (ionic radius 0.132 nm) sites of the SnO_2 , as defined by Bragg's equation ($n\lambda = 2d\sin\theta$) [7,17]. The results suggest that the peak intensities of (200) and (211) planes tend to gradually grow from FTO-10 Ω to FTO-3 Ω , demonstrating an improvement of the FTO crystallinity resulting from grain growth by the increased thickness of the FTO films [17,18], which is proved by the increased values of the grain sizes (~ 28.3 nm for FTO-10 Ω , ~ 32.5 for FTO-6 Ω , and ~ 33.7 nm for FTO-

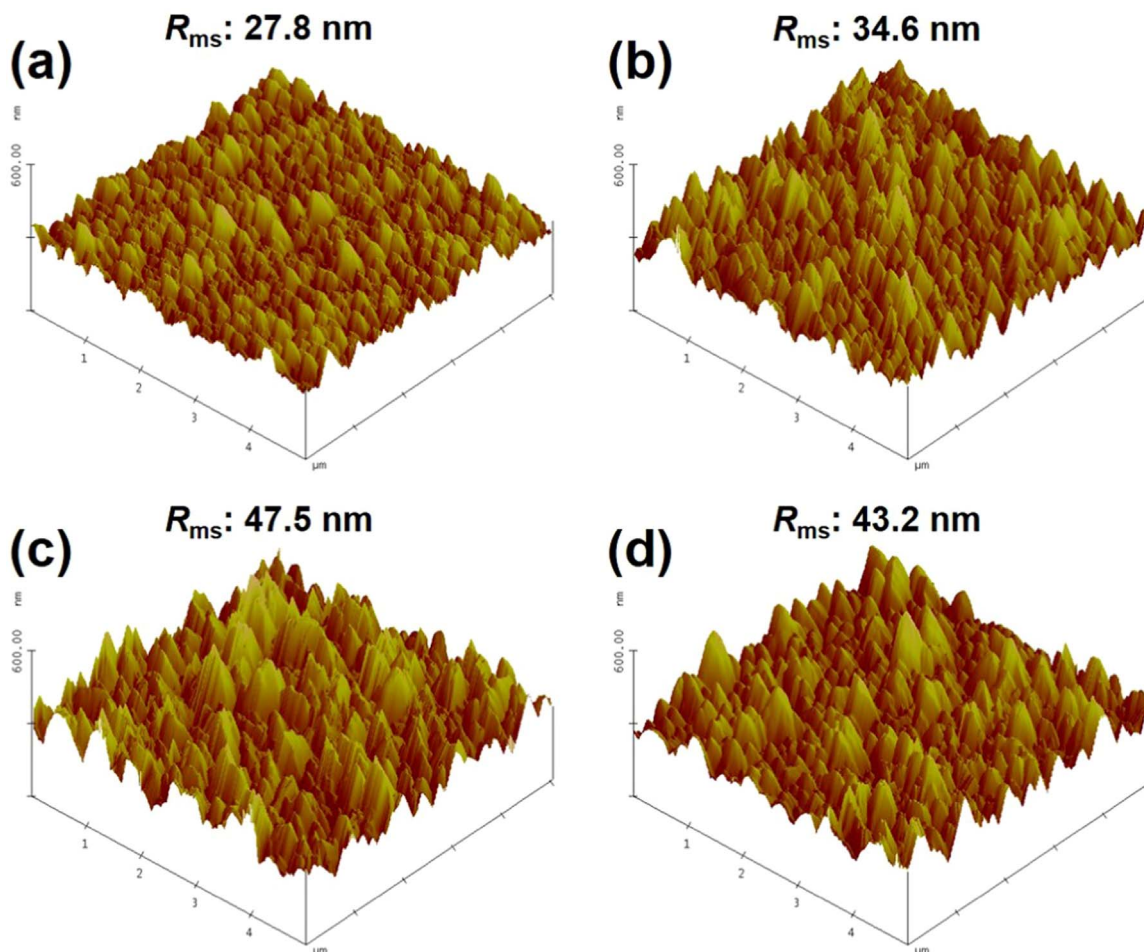


Fig. 2. AFM images of the surface obtained from (a) FTO-10 Ω , (b) FTO-6 Ω , (c) FTO-3 Ω , and (d) commercial FTO, respectively.

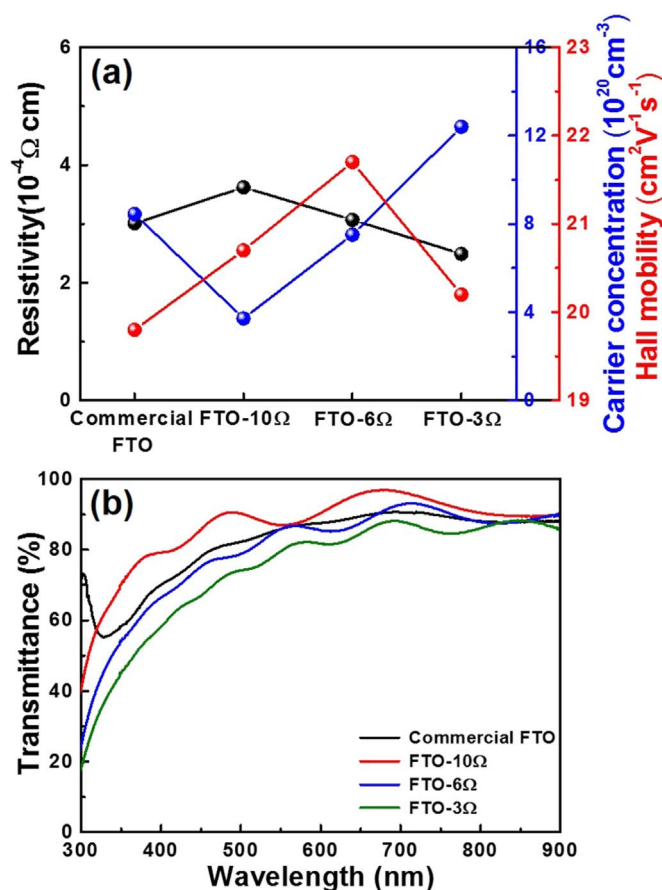


Fig. 4. (a) Electrical properties including carrier concentration, Hall mobility, and resistivity and (b) optical transmittance curves of all FTO films measured in wavelength range from 300 to 900 nm.

3 Ω) calculated using Scherrer equation ($D = 0.9\lambda/(\beta \cos\theta)$, where λ is the X-ray wavelength, β is the full width at half maximum, and θ is the Bragg angle) [19]. Interestingly, as compared to the commercial FTO (0.8), the FTO films formed by the HUSPD, especially FTO-10 Ω (2.3) and FTO-6 Ω (1.5), have the enhanced intensity ratio of (200)/(211) planes, indicating the formation of the FTO films with dominant (200) preferred orientations. This unique structure can be formed by a uniform film growth parallel to the substrate through horizontal supply of precursor droplets in the HUSPD system [10,20]. However, for FTO-3 Ω, the dominant growth of (211) plane is generated by the crystal reorientation effect caused due to a larger thickness of the FTO film [15], leading to the heterogeneous growth of the FTO films. Therefore, the formation of the uniform FTO films with (200) preferred orientations is successfully performed by using the HUSPD, which can lead to the efficient electron transport on the TCEs for performance improvement of ECDs [10,16,21].

Fig. 4a shows the electrical properties, including the carrier concentration, Hall mobility, and resistivity, of all FTO films. With an increase of the deposition time, the carrier concentration enhances from $3.72 \times 10^{20} \text{ cm}^{-3}$ for FTO-10 Ω to $7.51 \times 10^{20} \text{ cm}^{-3}$ for FTO-6 Ω and attain the maximum value of $12.40 \times 10^{20} \text{ cm}^{-3}$ at FTO-3 Ω. This is due to the improvement of crystallinity induced by the increased thickness of the FTO films [12,22]. In addition, the Hall mobility exhibits the increased value from $20.7 \text{ cm}^2/(\text{V s})$ for FTO-10 Ω to $21.7 \text{ cm}^2/(\text{V s})$ for FTO-6 Ω, which might be attributed to the combined effect of the larger crystallite size to relax the inter-grain boundary scattering and uniform surface morphology with (200) preferred orientations to efficiently transport the electron [16,24]. However, for FTO-3 Ω, the decreased Hall mobility ($20.2 \text{ cm}^2/(\text{V s})$) is observed due

to the formation of the rough surface morphology. Therefore, we obtained the resistivity (ρ) of the FTO films using the following equation (see Eq. (1)) [8]:

$$\rho = 1/(Ne\mu) \quad (1)$$

where N , μ , and e are carrier concentration, Hall mobility, and the electron charge ($1.60 \times 10^{-19} \text{ C}$), respectively. The resultant resistivity values (ρ) were $3.62 \times 10^{-4} \text{ Ω cm}$ for FTO-10 Ω, $3.07 \times 10^{-4} \text{ Ω cm}$ for FTO-6 Ω, and $2.49 \times 10^{-4} \text{ Ω cm}$ for FTO-3 Ω. Furthermore, sheet resistances of the FTO films obtained by considering the resistivity/thickness amounted to $10.3 \pm 0.42 \text{ Ω}/\square$ for FTO-10 Ω, $6.5 \pm 0.26 \text{ Ω}/\square$ for FTO-6 Ω, and $3.3 \pm 0.15 \text{ Ω}/\square$ for FTO-3 Ω, indicating that an increase of deposition time for the HUSPD causes an enhancement of the sheet resistance on the FTO films due to the major effect of the increased carrier concentration. For the average optical transmittances of the FTO films (see Fig. 4b), with an increase of deposition time of the HUSPD, decreased values from 90.4% for FTO-10 Ω to 79.1% for FTO-3 Ω are observed in the wavelength range of 400–800 nm. This decrease in the optical transmittance of the FTO films is attributed to the increasing thickness to rise a light scattering in the films [23]. In addition, the optical transmittance of EC electrodes consisting of WO₃ films and FTO films can vary according to the fundamental characteristic of the FTO films used as a TCE. As shown in Fig. 5, the absorbance at 633 nm, measured by deducting the baseline of each FTO film, slightly increased from WO₃-FTO-10 Ω to WO₃-FTO-6 Ω; however, WO₃-FTO-3 Ω exhibited a noticeable increase in the absorbance, which is because the heterogeneous growth of the FTO films causes an interfacial light-scattering between FTO and WO₃ [25]. Therefore, the electrical and optical properties of the FTO films (see Table 1) can be the important factor for improving the EC performances.

Fig. 6 shows the CV curves of all WO₃-FTO electrodes to characterize the electrochemical properties of FTO-10 Ω, FTO-6 Ω, FTO-3 Ω, and commercial FTO as a TCE for the ECDs. In all samples, one pair of the redox curve with the anodic and cathodic peaks is observed during the CV cycling, indicating that the EC characteristics of intrinsic WO₃ vary from deep blue in the colored state to transparent in the bleached state by reversibly performing the intercalation and deintercalation of Li⁺ and electron from the WO₃. Both anodic and cathodic current densities improved from WO₃-FTO-10 Ω to WO₃-FTO-3 Ω, suggesting an enhancement in the number of ions and electrons to diffuse and transfer into or out the WO₃ due to a decreased sheet resistance of the FTO films, indicating the increasing of electrochemical activity to affect the EC performance [26]. Interestingly, the anodic and cathodic current densities of FTO-6 Ω are higher than those of commercial FTO, despite similar values of sheet resistance ($6.5 \pm 0.26 \text{ Ω}/\square$ for FTO-6 Ω and $6.0 \pm 0.40 \text{ Ω}/\square$ for commercial FTO), which is attributed to efficient electron transport by (200) preferred orientations of FTO-6 Ω. This

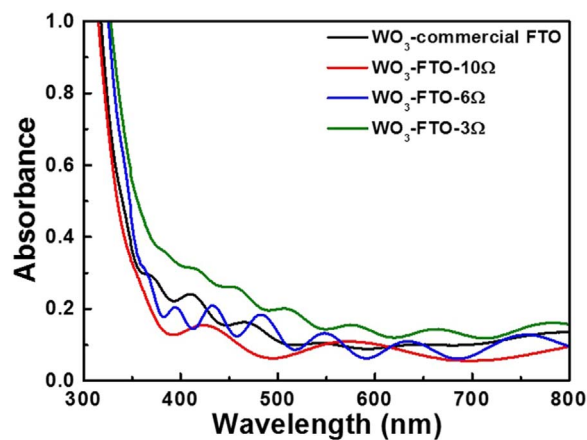


Fig. 5. Absorption spectra in wavelength range of 300–900 nm obtain from all WO₃-FTO electrodes.

Table 1
Summary of electrical and optical properties for all FTO films.

	Commercial FTO	FTO-10 Ω	FTO-6 Ω	FTO-3 Ω
Carrier concentration (cm^{-3})	8.45×10^{20}	3.72×10^{20}	7.51×10^{20}	12.40×10^{20}
Hall mobility ($\text{cm}^2/(\text{V s})$)	19.8	20.7	21.7	20.2
Resistivity ($\Omega \text{ cm}$)	3.01×10^{-4}	3.62×10^{-4}	3.07×10^{-4}	2.49×10^{-4}
Sheet resistance (Ω/\square)	6.0 ± 0.40	10.3 ± 0.42	6.5 ± 0.26	3.3 ± 0.15
Transmittance (%)	83.9	90.4	84.3	79.1

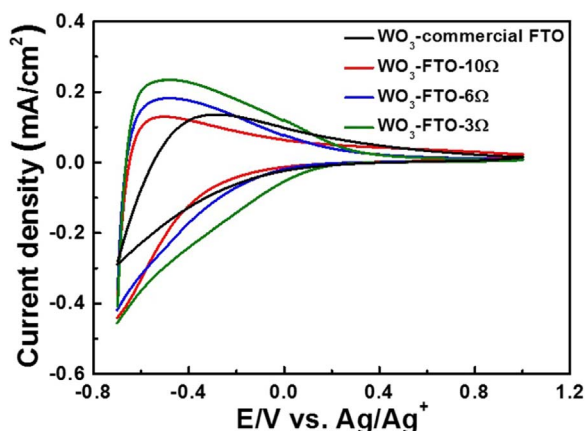


Fig. 6. CV curves of WO_3 -FTO-10 Ω , WO_3 -FTO-6 Ω , WO_3 -FTO-3 Ω , and WO_3 -commercial FTO.

implies that, as compared to commercial FTO, the FTO films fabricated using the HUSPD have enhanced electrochemical activity associated with good EC performance.

The *in situ* optical transmittances of the WO_3 -FTO electrodes at $\lambda_{633 \text{ nm}}$ were traced to monitor the EC responses of all FTO films by switching the potential between -0.7 for colored state and 1.0 V for the bleached state during 60 s. As shown in Fig. 7a, the curve of the *in situ* optical transmittances shows two information of transmittance modulation as defined as $\Delta T = T_b - T_c$ (T_b is transmittance in the bleached state and T_c is transmittance in the colored state) and switching speed defined as the time required to reach 90% of its full transmittance modulation at 633 nm (see Table 2). For the transmittance modulation, owing to the increased electrochemical activity to improve Li^+ intercalation and deintercalation, an increase in the values (from WO_3 -FTO-10 Ω (46.5%) to WO_3 -FTO-6 Ω (56.6%)) is observed. Then, there is a decreased transmittance modulation (53.3%) of WO_3 -FTO-3 Ω as compared to WO_3 -FTO-5 Ω despite their low sheet resistance due to a decreased transmittance in the bleached state by the high absorbance of WO_3 -FTO-6 Ω . The switching speeds are enhanced from WO_3 -FTO-10 Ω (13.1 s for coloration speed and 15.3 s for bleaching speed) to WO_3 -FTO-3 Ω (5.9 s for coloration speed and 4.3 s for bleaching speed), which is mainly related to the decreased sheet resistance of the FTO films. Therefore, the decrease of sheet resistance for the FTO films used as a TCE of the ECDs can be useful to accelerate the Li^+ and electron diffusion on the WO_3 films during intercalation/deintercalation processes [27]. Interestingly, as compared to WO_3 -commercial FTO (12.1 s for coloration speed and 13.9 s for bleaching speed), WO_3 -FTO-6 Ω exhibits a remarkable improvement of switching speeds (10.3 s for coloration speed and 8.9 s for bleaching speed), which can be induced by an efficient electron transport between FTO and WO_3 resulting from the dominant (200) preferred orientations of the FTO films formed by the HUSPD. This result is in accordance with the improvement of switching speed for the ECDs. In addition, the CE signifies a high sensitivity of the EC process, which defined as the optical density (OD) as a result of intercalated charge densities (Q/A) (see Eqs. (2) and (3)) [28]:

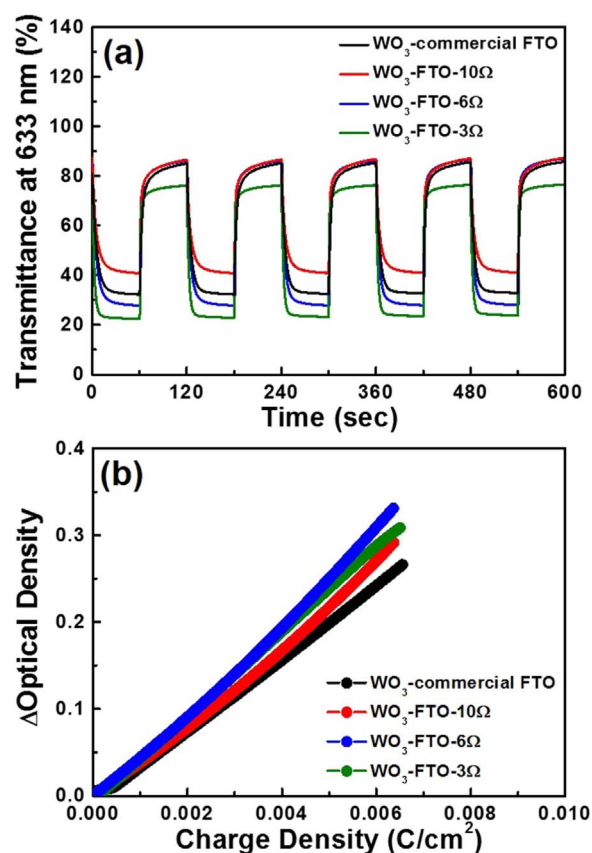


Fig. 7. (a) *In situ* optical transmittances spectra of the EC electrodes with all FTO films applied with an interval of 60 s at the potential of -0.7 for colored state and 1.0 V for bleached state and (b) variation of OD at 633 nm with intercalated charge density at -0.7 V.

$$\text{CE} = \Delta\text{OD}/(Q/A) \quad (2)$$

$$\Delta\text{OD} = \log(T_b/T_c) \quad (3)$$

where Q is the integration of the current within the colored time and A is the given electrode area, indicating that capable ECDs possess a high CE value. Fig. 7b shows the OD curve at the wavelength of 633 nm with the intercalated charge density at the potential of -0.7 V. The CE values calculated from the slope of the curve show that, despite the difference of sheet resistance on the FTO films, WO_3 -FTO-6 Ω represent a higher CE value than the other samples, which can be mainly attributed to the effect of a high transmittance modulation by the FTO films with the uniform surface morphology to reduce interfacial light-scattering between FTO and WO_3 . Therefore, our results demonstrate that WO_3 -FTO-6 Ω possesses the optimum EC performances, including the enhanced switching speeds (10.3 s for coloration speed and 8.9 s for bleaching speed) by the decrease in the sheet resistance of the FTO films and high CE ($50.9 \text{ cm}^2/\text{C}$) caused by the high transmittance modulation by uniform FTO films.

Table 2

Summary of EC performances measured from all WO₃-FTO electrodes.

Samples	T _b (%)	T _c (%)	Transmittance modulation (%; 633 nm)	Coloration speed (s)	Bleaching speed (s)	CE (cm ² /C)
WO ₃ -commercial FTO	85.0	32.5	52.5	12.1	13.9	37.2
WO ₃ -FTO – 10 Ω	87.3	40.8	46.5	13.1	15.3	43.3
WO ₃ -FTO – 6 Ω	86.1	29.5	56.6	10.3	8.9	50.9
WO ₃ -FTO – 3 Ω	76.1	22.8	53.3	5.9	4.3	48.0

4. Conclusion

The FTO films with three types of sheet resistances ($\sim 10 \Omega/\square$, $\sim 6 \Omega/\square$, and $\sim 3 \Omega/\square$) were fabricated by adjusting the deposition time of the HUSPD. For the HUSPD, it is useful to form a uniform film structure by the horizontal supply of precursor droplets, resulting in the uniform FTO films with (200) preferred orientations. With an increase of the deposition times of the HUSPD, the crystallite size and thickness on the FTO films were gradually enhanced, which led to a decrease of their sheet resistance due to the improved carrier concentration while the optical transmittances were dropped by the thickened thickness. As a result, the EC electrodes fabricated with the FTO films showed an acceleration of the switching speeds with a decrease of their sheet resistance to enhance the electrochemical activity. In addition, for the CE, despite the difference of the sheet resistance values, WO₃-FTO-6 Ω had a higher value than the other samples, which can be related to the high transmittance modulation induced from reduction of interfacial light-scattering between FTO and WO₃ by uniform surface morphology. Therefore, the results of the present study provide a valuable insight into the TCEs to improve the performance of the ECDs.

Acknowledgements

None.

References

- [1] Y. Ren, Y. Gao, G. Zhao, Facile single-step fabrications of electrochromic WO₃ micro-patterned films using the novel photosensitive sol–gel method, *Ceram. Int.* 41 (2015) 403–408.
- [2] K. Tajima, M. Ikeyama, S. Nakao, Y. Yamada, K. Yoshimura, Si incorporated diamond-like carbon film-coated electrochromic switchable mirror glass for high environmental durability, *Ceram. Int.* 39 (2013) 8273–8278.
- [3] W. Dong, Y. Lv, L. Xiao, Y. Fan, N. Zhang, X. Liu, Bifunctional MoO₃–WO₃/Ag/MoO₃–WO₃ films for efficient ITO-free electrochromic devices, *ACS Appl. Mater. Interface* 8 (2016) 33842–33847.
- [4] B.-R. Koo, H.-J. Ahn, Fast-switching electrochromic properties of mesoporous WO₃ films with oxygen vacancy defects, *Nanoscale* 9 (2010) 17788–17793.
- [5] G. Cai, J. Wang, P.S. Lee, Next-generation multifunctional electrochromic devices, *Acc. Chem. Res.* 49 (2016) 1469–1476.
- [6] Y.X. Wei, Y.B. Ma, M. Chen, W.M. Liu, L. Li, Y. Yan, Electrochemical investigation of electrochromic device based on WO₃ and Ti doped V₂O₅ films by using electrolyte containing ferrocene, *J. Electroanal. Chem.* 807 (2017) 45–51.
- [7] A.R. Babar, S.S. Shinde, A.V. Moholkar, C.H. Bhosale, J.H. Kim, K.Y. Rajpure, Physical properties of sprayed antimony doped tin oxide thin films: the role of thickness, *J. Semicond.* 32 (2011) 053001.
- [8] B.-R. Koo, J.-W. Bae, H.-J. Ahn, Low-temperature conducting performance of transparent indium tin oxide/antimony tin oxide electrodes, *Ceram. Int.* 43 (2017) 6124–6129.
- [9] H. Kim, G.P. Kushto, R.C.Y. Auyeung, A. Piqué, Optimization of F-doped SnO₂ electrodes for organic photovoltaic devices, *Appl. Phys. A* 93 (2008) 521–526.
- [10] B.-R. Koo, D.-H. Oh, D.-H. Riu, H.-J. Ahn, Improvement of transparent conducting performance on oxygen-activated fluorine-doped tin oxide electrodes formed by horizontal ultrasonic spray pyrolysis deposition, *ACS Appl. Mater. Interface* 9 (2017) 44584–44592.
- [11] T. Maruyama, H. Akagi, Fluorine-doped tin dioxide thin films prepared by radio-frequency magnetron sputtering, *J. Electrochem. Soc.* 143 (1996) 283–287.
- [12] N. Noor, I.P. Parkin, Enhanced transparent-conducting fluorine-doped tin oxide films formed by aerosol-assisted chemical vapour deposition, *J. Mater. Chem. C* 1 (2013) 984–996.
- [13] C.-C. Lin, M.-C. Chiang, Y.-W. Chen, Temperature dependence of fluorine-doped tin oxide films produced by ultrasonic spray pyrolysis, *Thin Solid Films* 518 (2009) 1241–1244.
- [14] A.V. Moholkar, S.M. Pawar, K.Y. Rajpure, C.H. Bhosale, Effect of concentration of SnCl₄ on sprayed fluorine doped tin oxide thin films, *J. Alloy. Compd.* 455 (2008) 440–446.
- [15] A. Nadarajah, M.E. Carnes, M.G. Kast, D.W. Johnson, S.W. Boettcher, Aqueous solution processing of F-doped SnO₂ transparent conducting oxide films using a reactive tin(II) hydroxide nitrate nanoscale cluster, *Chem. Mater.* 25 (2013) 4080–4087.
- [16] K. Murakami, I. Yagi, S. Kaneko, Oriented growth of tin oxide thin films on glass substrates by spray pyrolysis of organotin compounds, *J. Am. Ceram. Soc.* 79 (1996) 2557–2562.
- [17] D. Kashchiev, Growth of crystallites in deposition from vapours, *Phys. Stat. Sol.* 64 (1981) 715–721.
- [18] A.V. Moholkar, S.M. Pawar, K.Y. Rajpure, P.S. Patil, C.H. Bhosale, Properties of highly oriented spray-deposited fluorine-doped tin oxide thin films on glass substrates of different thickness, *J. Phys. Chem. Solids* 68 (2007) 1981–1988.
- [19] B.-R. Koo, H. An, H.-J. Ahn, High-surface area co-electrospun TiO₂ nanowires fabricated using shrinkage of polyvinylpyrrolidone for improved photovoltaic performance, *Ceram. Int.* 42 (2016) 1666–1671.
- [20] B.-R. Koo, D.-H. Oh, H.-J. Ahn, Influence of Nb-doped TiO₂ blocking layers as a cascading band structure for enhanced photovoltaic properties, *Appl. Surf. Sci.* 433 (2018) 27–34.
- [21] Y.D. Wang, I. Djerdj, M. Antonietti, B. Smarsly, Polymer-assisted generation of antimony-doped SnO₂ nanoparticles with high crystallinity for application in gas sensors, *Small* 4 (2008) 1656–1660.
- [22] J.H. Park, S. Jang, D. Byun, J.K. Lee, Fluorine doped gallium tin oxide composite films as transparent conductive oxides on polyethylene terephthalate film prepared by electron cyclotron resonance metal organic chemical vapor deposition, *Thin Solid Films* 519 (2011) 6863–6867.
- [23] E. Elangovan, K. Ramamurthi, A study on low cost-high conducting fluorine and antimony-doped tin oxide thin films, *Appl. Surf. Sci.* 249 (2005) 183–196.
- [24] A.V. Moholkar, S.M. Pawar, K.Y. Rajpure, C.H. Bhosale, J.H. Kim, Effect of fluorine doping on highly transparent conductive spray deposited nanocrystalline tin oxide thin films, *Appl. Surf. Sci.* 255 (2009) 9358–9364.
- [25] S.H. Kang, J.-Y. Kim, H.S. kim, H.-D. Koh, J.-S. Lee, Y.-E. Sung, Influence of light scattering particles in the TiO₂ photoelectrode for solid-state dye-sensitized solar cell, *J. Photochem. Photobiol. A-Chem.* 200 (2008) 294–300.
- [26] M. Wang, Q. Liu, G. Dong, Y. He, X. Diao, Influence of thickness on the structure, electrical, optical and electrochromic properties of AZO thin films and their inorganic all-solid-state devices, *Electrochim. Acta* 258 (2017) 1336–1347.
- [27] A. Hagfeldt, N. Vlachopoulos, M. Grätzel, Fast electrochromic switching with nanocrystalline oxide semiconductor films, *J. Electrochem. Soc.* 141 (1994) L82–L84.
- [28] C.-K. Wang, C.-K. Lin, C.-L. Wu, S. Brahma, S.-C. Wang, J.-L. Huang, Characterization of electrochromic tungsten oxide film from electrochemical anodized RF-sputtered tungsten films, *Ceram. Int.* 39 (2013) 4293–4298.